

Observation of deterministic double dissipative-Kerr-soliton generation with avoided mode crossing

Hao Liu^{1,*}, Wenting Wang^{1,2,†}, Jinghui Yang¹, Mingbin Yu³, Dim-Lee Kwong³, and Chee Wei Wong^{1,‡}

¹Fang Lu Mesoscopic Optics and Quantum Electronics Laboratory, University of California Los Angeles, California 90095, USA

²Communication and Integrated Photonics Laboratory, Xiongan Institute of Innovation, Chinese Academy of Sciences, Xiong'an New Area 071700, China

³Institute of Microelectronics, Singapore 138634, Singapore



(Received 23 February 2022; accepted 9 December 2022; published 13 March 2023)

Dissipative Kerr solitons (DKSs) in microresonators have boosted the development of the chip-scale ultra-stable microcomb sources, and thrived in both fundamental physics and a wide range of applications. Among various DKS states, single DKS, double DKS, and a perfect soliton crystal could be identified simply based on the optical spectrum. Especially, the double DKS state, due to its two-pulse-interference nature, has recently found its own application in microwave photonics, such as reconfigurable rf filters. However, the traditional method to generate double DKS usually yields stochastically relative positions of the DKS in the cavity, which limits the versatility of the application. Here a method to deterministically generate double DKSs with fixed relative positions assisted by the dual-pump driven scheme in a 97-GHz Si₃N₄ microresonator is demonstrated. Via the dual-pump scheme, not only has the single soliton been repeatably generated, double DKS with deterministic relative positions has also been realized through backward tuning. The effects of pump wavelength tuning and pump power on the relative positions are investigated. A direct bridge between the relative positions and the avoided mode crossing induced modulated cw background is established. This work not only provides insight to DKS dynamics in a dual-pump scheme, but also improves the versatility of double-DKS based applications in microwave photonics.

DOI: [10.1103/PhysRevResearch.5.013172](https://doi.org/10.1103/PhysRevResearch.5.013172)

Over the past decade, remarkable breakthroughs have been seen in the chip-scale frequency microcomb studies with ultrahigh- Q microresonators [1–7], from table-top demonstrations [8,9] to small factor integrated platforms [10–12], thriving in both fundamental dynamics [9,13–20] and various applications, including spectroscopy [21], optical coherent tomography (OCT) [22,23], low noise radio frequency generation [24,25], frequency synthesis [10], distance ranging [26,27], photonic convolution processing [28,29], and high-speed optical communication [30–32]. Among these studies, dissipative Kerr solitons (DKSs), which require a delicate balance between loss and parametric gain, as well as Kerr nonlinear phase shift and anomalous dispersion [33], draw the most attention, for their broadband optical frequency comb nature. DKS states include single DKS, multi-DKS, and soliton crystal [34] states. Except for the single DKS state, which has a sech^2 envelope, all the other DKS states' optical spectra are just the interference of several soliton pulses circulating around the cavity. The comb line intensity

could be expressed as [7] $I(\mu) = |\sum_{j=1}^N \exp(i\phi_j\mu)|^2$, where ϕ is the phase of each comb line, while μ is the comb line number. However, except for perfect soliton crystal states [35] and double DKS states, other multi-DKS states are difficult to identify merely from the spectra. Recently, the lotuslike double DKS state, due to its interference nature, has found its own application in the microwave photonics area. However, although repeatable double DKS generation is realized, the relative position (hereafter we use the term azimuthal angle to describe it) between the two soliton pulses is still stochastic [36].

Here we experimentally demonstrate a method to deterministically generate double DKS with fixed azimuthal angle assisted by the dual-pump driven scheme in a 97-GHz Si₃N₄ microresonator. The Si₃N₄ platform is currently the most widely applied platform due to its complementary metal-oxide semiconductor-compatible fabrication process, large Kerr nonlinearity, broad transparent window, low Raman nonlinearity, and high-power handling capability [33]. However, just like the other platforms, such as AlGaAs, AlN, Si, and SiO₂, Si₃N₄ also suffers from the thermal effect, which makes it difficult to tune the pump laser to the effective red-detuned regime, where DKS states exist. In order to mitigate the fast thermal effect, power kicking [37] and high-speed frequency scanning [38] methods are proposed with abrupt change of power or frequency to bypass the thermal effect. The emergence of the dual-pump scheme significantly simplifies the procedure to generate the single DKS state [39,40]. With the assistance of an auxiliary pump at the C band, the nonlinear

*Corresponding author: haoliu1991@ucla.edu

†Corresponding author: wenting.wang@xii.ac.cn

‡Corresponding author: cheewei.wong@ucla.edu

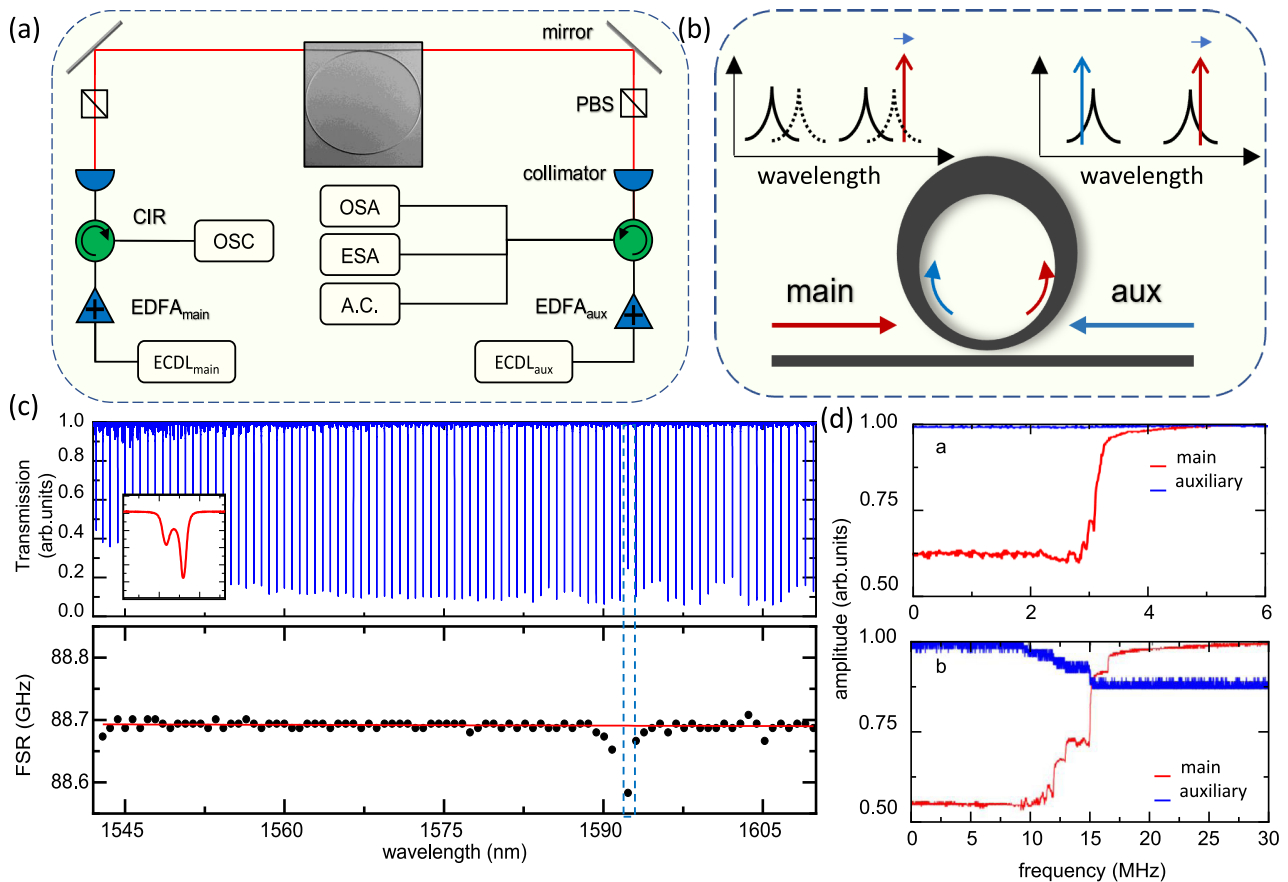


FIG. 1. Deterministic double dissipative-Kerr-soliton generation. (a) Schematic setup of dual-pump driven soliton generation. The main pump and the auxiliary pumps are launched into the 97-GHz Si_3N_4 microresonator in counterpropagating directions and separated via circulators (CIR). Both the main pump and the auxiliary pump are selected at TE polarization with polarizing beam splitter (PBS). The reflection path of the circulator on the auxiliary side is utilized for optical spectrum, amplitude noise, and autocorrelation (A.C.) measurements. The reflection of the other circulator is used for monitoring the transmission of the auxiliary pump. OSC: oscilloscope; OSA: optical spectrum analyzer; ESA: electronic spectrum analyzer. (b) Scheme of dual-pump driven method. The main pump and the auxiliary pump are launched into the microresonator in the opposite direction. The upper left inset depicts single pump scheme, in which resonances will shift to shorter wavelengths when the pump is at effective red-detuned regime. The upper right inset illustrates the dual-pump scheme, in which all the resonances remain at the same position, when the main pump is tuned in the effective red-detuned regime, with the auxiliary pump set at the effective blue-detuned regime. (c) Device characterization. Upper panel depicts the transmission of the tested 97-GHz Si_3N_4 microresonator. The inset shows the inevitable TE-TM mode coupling. The lower panel illustrates the FSRs of the resonances across 65 nm, with fitted anomalous GVD of $-7 \text{ fs}^2/\text{mm}$. The dashed blue box circles the AMX attributed to the TE-TM mode coupling. (d) Pump power transmission of both pumps in single pump scheme and dual-pump regime. The upper panel shows that without the auxiliary pump, the soliton characteristic steps only maintain over tens of kHz. The lower panel illustrates that with the presence of the auxiliary pump, the soliton characteristic step is significantly extended to several MHz. Both measurements are implemented with laser scanning speed of 2.5 THz/s.

thermal effect of Si_3N_4 is significantly mitigated, hence the effective red-detuned regime could be easily accessed through manual wavelength tuning. Then a 97-GHz single DKS is repeatedly accessed, confirmed by the sech^2 optical spectrum shape, the amplitude noise measurement, as well as the autocorrelation measurement. Furthermore, several double DKS states are demonstrated with different azimuthal angles. Next, we report a deterministic method to generate double DKS states with fixed azimuthal angle, directly accessed from the single DKS state, with backward detuning. The fine tuning of the azimuthal angle via wavelength tuning and pump power variation are further investigated. Finally, the connection between the deterministic coarse dialing of double DKS states with different angles from 180° to 17° and the avoided mode crossing (AMX) is established.

Figure 1(a) demonstrates the schematic setup of the dual-pump driven method for single and double DKS generation. In the experiment, a Si_3N_4 planar microresonator with 800 nm height is utilized for DKS generation. The width of the microresonator is tapered from 4 to 1 μm , where the light is coupled out to the bus waveguide. Unlike the common uniform waveguide design, such taper design could effectively suppress higher order mode family, averting avoided mode crossing (AMX) induced by the coupling between different transverse mode families [41]. Furthermore, the taper design could also achieve a higher Q factor as well as offer an extra degree of freedom to engineer the net dispersion, which are discussed in our previous works [42]. Figure 1(c) shows the cold cavity transmission of the 97-GHz microresonator. A high speed swept wavelength interferometer is applied to

record more than 100 TE_{00} resonances over the whole C and L bands, with loaded Q factors higher than 1.5 million. The lower panel plots the free spectral range (FSR) of all the recorded resonances, with retrieved group velocity dispersion (GVD) of $-7 \text{ fs}^2/\text{mm}$. The discontinuity of the FSR in the blue dashed box indicates the AMX originating from the inevitable coupling between TE and TM mode families. A detailed depiction of the related resonance is in the lower left of the upper panel. Such AMX is critical in the deterministic double DKS generation, and will be discussed in detail later in this paper.

The dual-pump driven method in our implementation utilizes two external cavity diode lasers (ECDLs), which are amplified by two Er-doped fiber amplifiers (EDFAs) and then launched in to the microresonator in counterpropagating directions. Both pumps are selected in TE polarization with polarized beam splitters (PBSs), due to anomalous dispersion and higher Q factor in TE mode. First, the auxiliary pump (ECDL_{aux}) is tuned, from shorter wavelength to longer wavelength, into a resonance in C band (around 1565 nm in our case), and then stopped at the effective blue-detuned regime. Then the main pump (ECDL_{main}) is launched into a resonance at around 1598 nm in the counterpropagating direction. Since both pumps are in the same polarization, in order to collect the transmission power of both main and auxiliary pumps, two high-power circulators are utilized. The reflection port of the left circulator in Fig. 1(a) is used for monitoring the tuning of the auxiliary pump, while the reflection port of right circulator is split into three paths for optical spectrum, amplitude noise, and autocorrelation measurements. Figure 1(b) shows the scheme of the dual-pump driven method. The upper left is the scenario that only involves a single pump. The detuning between pump laser and the resonance is usually defined as $\Delta = \omega_0 - \omega_p$, where ω_0 is the angular frequency of the cold cavity pump resonance and ω_p is the angular frequency of the pump laser. In the presence of thermal effect, an extra resonance shift introduced to the pump resonance frequency is approximately proportional to the product of the Q factor of the resonance and the power coupled to the cavity: $\Delta_T \propto QP_c$, where $\Delta_T = \omega_0 - \omega'_0$ is the thermally induced resonance shift with the effective resonance frequency ω'_0 , Q is the quality factor of the pump resonance, and P_c is the power coupled into the pump resonance from the pump laser. Then the effective detuning could be written as $\Delta_{\text{eff}} = \omega_0 - \omega_p - \Delta_T$. When only a single pump is forwardly (shorter wavelength to longer wavelength) tuned into a resonance at the effective blue-detuned regime, due to the positive thermal-refractive coefficient in Si_3N_4 , the resonance tends to shift to lower frequency (longer wavelength) as there is more power coupled into the resonance, and the effective detuning tends to become longer than without thermal effect. However, when pump laser is in the effective red-detuned regime, where DKS states exist, the pump resonance shifts to higher frequency (shorter wavelength) in forward tuning, which makes the effective detuning region much shorter than without thermal effect. Such phenomenon results in the thermal triangle in the pump scanning measurement [43].

Figure 1(d) upper panel plots the transition of the thermal triangle with the presence of a single pump. The characteristic step for DKS states is on the hundreds of kilohertz level

when the pump is scanned at a scanning speed of 2.5 THz/s, which makes it extremely difficult to generate DKS states with manual tuning. In the presence of the auxiliary laser, the thermal induced resonance shift is dominated by both pump, i.e., $\Delta_T \propto Q_{\text{main}}P_{\text{main}_c} + Q_{\text{aux}}P_{\text{aux}_c}$, where Q_{aux} is the quality factor of the auxiliary pump resonance, and P_{aux_c} is the power coupled from the auxiliary pump. Since the auxiliary pump is set at the blue-detuned regime of the picked resonance, when the main pump is forwardly tuned into the resonance at the blue-detuned regime, P_{main_c} increases and tends to redshift all the resonances, then the auxiliary pump is equivalently tuned away from the resonance, hence P_{aux_c} decreases, then Δ_T is mitigated. And when the main pump is forwardly tuned at the red-detuned regime, P_{main_c} decreases and all the resonances tend to be blueshifted, so that the auxiliary pump is equivalently tuned towards the resonance, hence P_{aux_c} increases, then Δ_T is mitigated. So the resonance will remain unchanged during the main pump tuning, with the appropriate choice of auxiliary resonance and auxiliary pump power. In result, the resonances are thermally stabilized by the auxiliary pump. With the help of the thermal stabilization of the auxiliary pump and the cross-phase modulation (XPM) between the main and auxiliary pumps, the increase of effective detuning at the red-detuned regime is retarded, which manifests itself as a much longer characteristic step of DKS states during the pump transmission measurement at the same scanning speed. The lower panel of Fig. 1(d) shows the corresponding measurement, from which we could see that the characteristic step is at the several MHz level, which is boosted by more than 30 times. Such an elongated characteristic step makes manually tuned DKS states possible.

Via a forward tuning, the comb evolution starts from the primary comb line, and goes through the Turing pattern, chaotic combs, and arrives at stable DKS states. With the careful choice of the auxiliary resonance and auxiliary pump power, the evolution in the DKS states will repeatedly arrive at single DKS state, from multisoliton states. Figure 2(a) is the optical spectrum of a single DKS state with signature sech^2 shape. The low noise state is confirmed with amplitude noise measurement up to 1 GHz, which is shown in the upper left inset. Furthermore, we implemented a nonlinear autocorrelation measurement on the single DKS state, as shown in Fig. 2(b). The setup for soliton generation is connected to the autocorrelation setup via a long fiber link. Although the fiber link is not optimized for zero link dispersion, which causes inevitable broadening of the soliton pulse width, the single pulse wave form with 10.24-ps period further confirms a 97-GHz single DKS generation.

Figure 2(c) shows a typical double DKS state with recognizable interference pattern. Through autocorrelation measurement shown in Fig. 2(d), the time interval between the two solitons in the double DKS state is 0.86 ps. The retrieved azimuthal angle with respect to the 10.24-ps period is 30° . Figure 2(e) shows a unique double DKS state with azimuthal angle of 180° . The exact π phase difference results in a double FSR comb spectrum. Figure 2(f) shows another double DKS state with azimuthal angle of 21° , which has a significantly wider lobe size than the 30° case. In the evolution process from multi-DKS states to single DKS state, the pulses circulating along the microcavity diminish

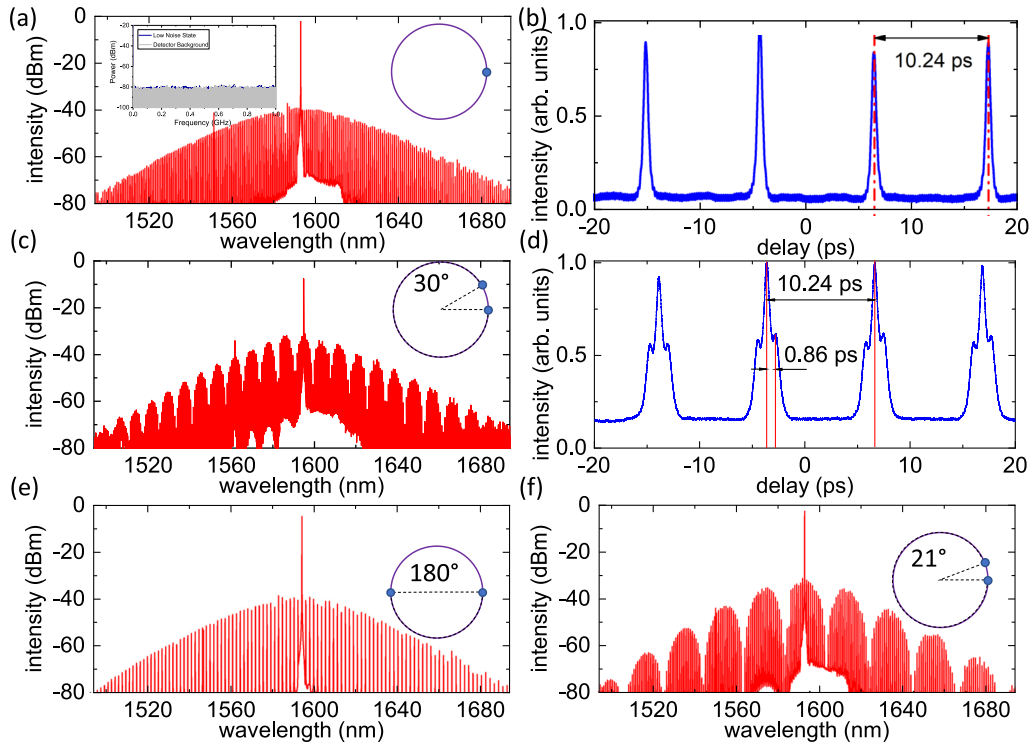


FIG. 2. DKS generation via dual-pump driven method. Schematic depiction of DKS distribution along the microresonator is shown on the upper right of each optical spectrum. (a) Single DKS optical spectrum. The upper left inset is the amplitude noise measurement (blue curve) of the DKS state compared with the detector background noise (gray curve). (b) Autocorrelation of the single DKS state. The 10.24-ps period proves the 97-GHz single pulse generation. (c) A double DKS state with azimuthal angle of 30° . (d) Autocorrelation measurement of the double DKS state in (c). The 0.86-ps spacing between the peaks illustrates the 30° separation of the two pulses. (e) Another typical double DKS state with azimuthal angle of 180° . Due to the 180° azimuthal angle between the two pulses, the interference results in a double-FSR comb spectrum. (f) A double DKS state with azimuthal angle of 21° . As the azimuthal angle decreases, the interference envelope would have a wider lobe width, which is a good indicator to roughly compare the azimuthal angle.

consecutively. Hence, theoretically a double DKS state could always be achieved in each comb evolution. However, the detuning range for each DKS state could vary in each evolution, consequently, the double DKS state cannot be generated in every trial. Furthermore, since the position of the pulses in the cavity is regulated by the modulated background due to the interference between the pump and the AMX, the azimuthal angle of the double DKS state is also stochastic [36].

In the presence of the auxiliary pump, bidirectional switching could be realized, similar to the photorefractive effect [44] in the LiNbO₃ platform. Unlike previous work [45] in which backward tuning causes pulse number changing from a higher number to a lower number, the thermal stabilization via auxiliary pump could realize not only a soliton burst [39], but also realize an ascending switch of soliton numbers. Here in our work, we did not focus on a soliton burst but we focused on the DKS state switching from a single DKS state during backward tuning. Particularly, we found out that once the single DKS state is achieved, if one slowly tunes the main pump wavelength backwardly, the comb will always arrive at a double DKS state with the same azimuthal angle in a deterministic fashion, when the pump power and resonance are not changed. Since the double DKS states have a recognizable modulated pattern due to the interference between the two soliton pulses, it is rather easy to retrieve the azimuthal angle from fitting. Hence, all the azimuthal angle information

hereafter is retrieved from the spectral fitting of the double DKS state.

In our experiments we notice that the main and auxiliary pump intensities need to be carefully chosen to achieve single DKS to double DKS switching. In our experimental scheme, the auxiliary pump is set at 27 dBm, and only when the main pump power is between 23 and 25 dBm could the deterministic double DKS generation be realized. Although the azimuthal angle between the two solitons in the double DKS state is fixed via backward tuning, it could still be slightly tuned through forward tuning. Figures 3(a)–3(c) show the experimental results for the azimuthal angle tuning through forward tuning. First, the comb is manually tuned into a single DKS state, then a slow manual backward tuning is applied to the main pump until a double DKS state with azimuthal angle of 21° is achieved. Next, the main pump wavelength is slowly tuned forwardly, until a single DKS state is arrived at again. During the process, double DKS states with azimuthal angles of 18° and 17° are captured through an OSA, consecutively. However, since the forward tuning is applied manually and the OSA has a relatively slow capture time, a continuous variation of the azimuthal angle is not recorded, nor is the smallest azimuthal angle observed.

This is due to the modulated background from the AMX. As mentioned previously, the pulse azimuthal position is regulated by the modulation on the cw background introduced

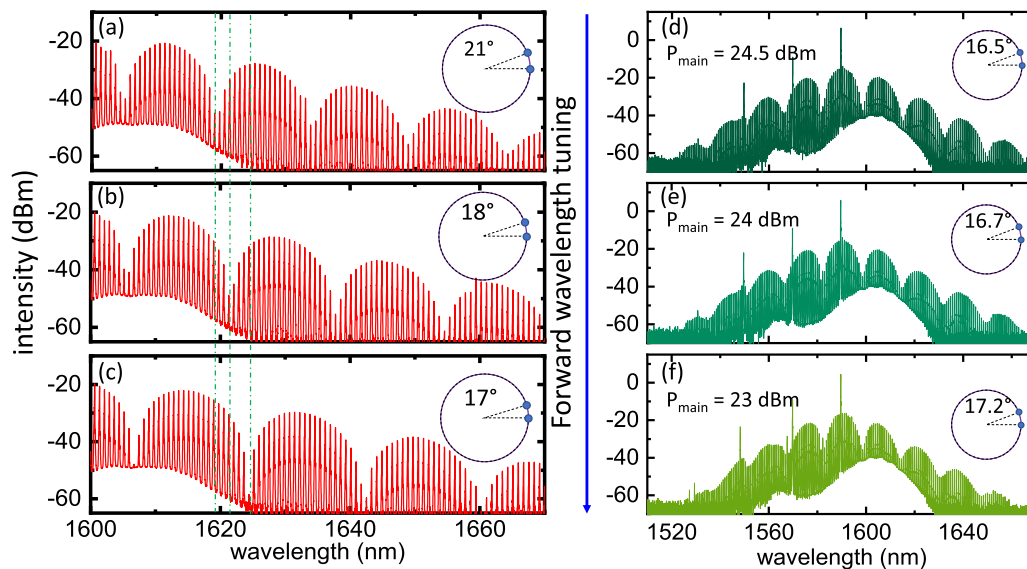


FIG. 3. Deterministic generation of double DKS and azimuthal angle control. (a)–(c) azimuthal angle of double DKS tuning through pump wavelength tuning. The azimuthal angle between the two DKS pulses tends to decrease as forward wavelength tuning. Through finely and slowly tuning of the wavelength, the azimuthal angle is deterministically controlled over 4° , where the green dashed lines show the power variations of comb lines due to the pulse interference. (d)–(f) azimuthal angle of double DKS tuning through pump power control. As the main pump power decreases from 24.5 to 23 dBm, the azimuthal angle is slightly increased by 0.7° . The azimuthal angle is 16.5° in (d), 16.7° in (e), and 17.2° in (f).

by the AMX. The time period of the modulated background is directly related to the frequency difference between the pump resonance and the maximum mode shift resonance. The larger the frequency difference, the shorter the time period. Hence, during the forward tuning, as the frequency difference is increasing, the time interval of two adjacent potential wells that could trap the soliton pulses gets closer. Therefore, the azimuthal angle in the double DKS state shows a descending trend along with forward tuning. Similarly, Once the deterministic double DKS is realized, by changing the main pump power, the azimuthal angle could also be tuned slightly. Figures 3(d)–3(f) plot the corresponding measurement results. In the similar auxiliary pump scheme, the main pump is set at 24.5 dBm. In the same procedure, we obtain a double DKS state with azimuthal angle of 16.5° . When the main pump power is decreased to 24 dBm, the azimuthal angle is then increased to 16.7° . Figure 3(f) shows that when the main pump is set at 23 dBm, the azimuthal angle is further increased to 17.2° . The azimuthal angle has an ascending trend as the pump power decreases.

Next, we investigated the relationship between the deterministic azimuthal angle and the pump position with respect to the maximum mode shift induced by AMX. Figure 4(a) depicts the accumulated dispersion D_{int} vs mode numbers. The abrupt change is induced by AMX. Here we define the pump mode as mode 0, and the mode number where the maximum mode shift happens as N . In Fig. 4(a), $N=11$, which means that the pump mode is 11 FSR away from the maximum mode shift induced by AMX. Figure 4(b) plots the optical spectrum of the double DKS state pumped at $N=11$, generated via the backward tuning procedure. The azimuthal angle is 17.14° in a deterministic fashion. The angle is retrieved from spectral fitting, as previously mentioned. The fitting curve is plotted in red line on top of the optical spectrum. Figure 4(c) plots the

deterministically generated double DKS state with azimuthal angle of 17.2° when $N=10$. Figures 4(d)–4(j) plot the double DKS states when $N=9, 6, 5, 4, 3, 2$, and 1. The azimuthal angles are $16.24^\circ, 33^\circ, 32.5^\circ, 46.75^\circ, 62.4^\circ, 63^\circ$, and 180° , respectively. Since the azimuthal angle in Fig. 4(j) is 180° , leading to a double-FSR comb spectrum, spectral fitting is not necessary and hence not plotted. Figure 4(k) summarizes the azimuthal angle for a double DKS state generated at different pump mode. Due to unknown reasons, there are no deterministic double DKS generations at pump modes 7 and 8. For the other cases, double DKS states are generated as expected. Overall, the azimuthal angle shows a descending trend as the pump mode is away from the resonance with maximum mode shift, which matches with our prediction, shown in the red curve. The prediction is based on a single AMX point using a two-parameter model, however, in real implementation, the auxiliary pump will also contribute to the modulation of the cw background, leading to a more complex background field. This could account for the deviation of the measurement from the prediction.

In conclusion, through a TE-TE dual-pump driven method, we demonstrate a scheme to deterministically generate a double DKS state with fixed azimuthal angle in a 97-GHz Si_3N_4 microresonator. Assisted by an auxiliary pump at the C band, the thermal nonlinearity is significantly mitigated. Hence, the characteristic steps for DKS states are elongated, so that single soliton state could be repeatedly generated manually, which was difficult to achieve with a single pump in our Si_3N_4 platform previously. Although no soliton burst is demonstrated in this work, we successfully observed bidirection switching, in which the soliton number decreases in forward tuning while it increases in backward tuning. Particularly, we demonstrated double DKS state generation through backward tuning from a single DKS state. Although a similar phenomenon has been

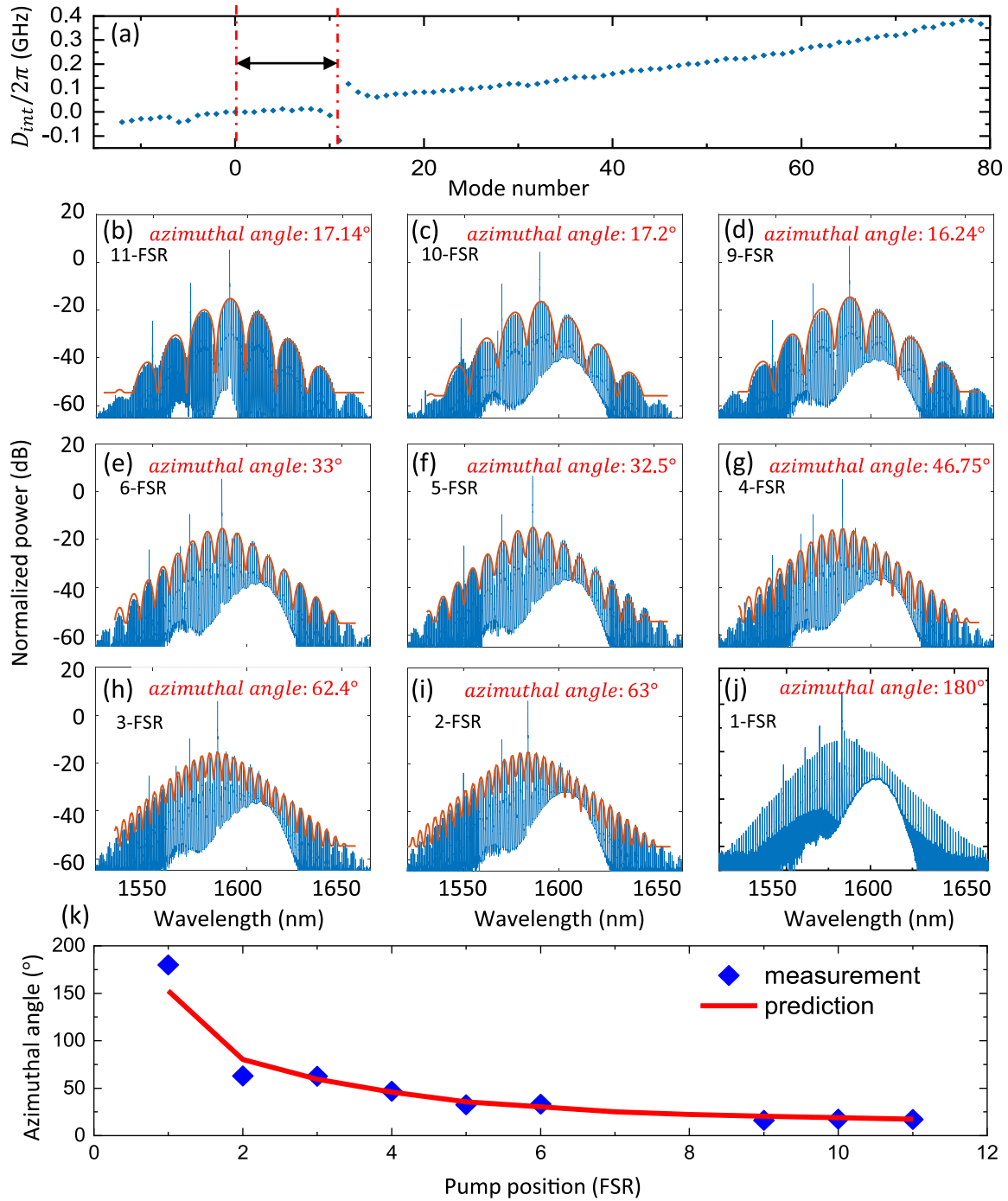


FIG. 4. Deterministic generation of double DKS with fixed azimuthal angle through AMX. (a) D_{int} vs mode number. The maximum AMX is located 11 FSR away from the pump mode (mode 0). (b)–(j) Optical spectra of different double DKS states pumped at different resonances with respect to the maximum AMX position. 11-FSR to 2-FSR cases show typical double DKS interference envelope, from which the azimuthal angles are fitted from the interference patterns. In the 1-FSR case, the optical spectrum shows a double FSR comb, indicating a 180° azimuthal angle. (k) Summary of the azimuthal angles in different pump position cases. The result shows clear descending trend of the azimuthal angle with respect to increasing pump-AMX spacing.

mentioned in a recent published paper [40] during the preparation of this manuscript, we focus on the double DKS state’s azimuthal angle control and establish a bridge between AMX and the azimuthal angle. In the backward tuning from a single DKS state, the comb always arrives at a double DKS state with deterministic azimuthal angle, when pumped at the same resonance. However, once the double DKS is generated, the

azimuthal angle could be fine-tuned through forward tuning or pump power control. The azimuthal angle tends to decrease in forward tuning and increase when the pump power decreases. Furthermore, we demonstrated that the deterministic azimuthal angle is directly related to the modulated cw background induced by AMX. Therefore, by choosing different pump resonance with respect to the maximum mode shift

that originates from AMX, we successfully dial the azimuthal angle from 180° to 17° . We believe that with appropriate control of the AMX, such as the method demonstrated in [46], the azimuthal angle could be further manipulated. This study not only enriches the understanding of DKS dynamics in a dual-pump driven scheme, but also offers more versatility of the double DKS state in the application of microwave photonics, such as microcomb based reconfigurable rf filters [36].

The authors thank for the fruitful discussions Dr. Y.-S. Jang, Dr. A. Vinod, and Prof. H. Zhou. This material was

based upon work supported by the Office of Naval Research (Grant No. N00014-16-1-2094), DARPA, and the National Science Foundation (Grants No. 1741707, No. 1810506, and No. 1824568).

H.L. designed the experiments and analyzed the data. H.L. and W.W. performed the experiments. J.Y. designed the resonator, and M.Y. and D.L.K. fabricated the microresonator. H.L. and C.W.W. prepared the manuscript. All authors contributed to discussion and revision of the manuscript.

-
- [1] B. J. M. Hausmann, I. Bulu, V. Venkataraman, P. Deotare, and M. Lončar, Diamond nonlinear photonics, *Nat. Photonics* **8**, 369 (2014).
- [2] H. Jung, C. Xiong, K. Y. Fong, X. Zhang, and H. X. Tang, Optical frequency comb generation from aluminum nitride microring resonator, *Opt. Lett.* **38**, 2810 (2013).
- [3] P. Del’Haye, A. Schliesser, O. Arcizet, T. Wilken, R. Holzwarth, and T. J. Kippenberg, Optical frequency comb generation from a monolithic microresonator, *Nature (London)* **450**, 1214 (2007).
- [4] T. Herr, V. Brasch, J. D. Jost, I. Mirgorodskiy, G. Lihachev, M. L. Gorodetsky, and T. J. Kippenberg, Mode Spectrum And Temporal Soliton Formation In Optical Microresonators, *Phys. Rev. Lett.* **113**, 123901 (2014).
- [5] M. Pu, L. Ottaviano, E. Semenova, and K. Yvind, Efficient frequency comb generation in algaas-on-insulator, *Optica* **3**, 823 (2016).
- [6] Y. He, Q.-F. Yang, J. Ling, R. Luo, H. Liang, M. Li, B. Shen, H. Wang, K. Vahala, and Q. Lin, Self-starting bi-chromatic linbo 3 soliton microcomb, *Optica* **6**, 1138 (2019).
- [7] V. Brasch, M. Geiselmann, T. Herr, G. Lihachev, M. H. P. Pfeiffer, M. L. Gorodetsky, and T. J. Kippenberg, Photonic chip-based optical frequency comb using soliton cherenkov radiation, *Science* **351**, 357 (2016).
- [8] S.-W. Huang, J. Yang, J. Lim, H. Zhou, M. Yu, D.-L. Kwong, and C. W. Wong, A low-phase-noise 18 GHz kerr frequency microcomb phase-locked over 65 THz, *Sci. Rep.* **5**, 13355 (2015).
- [9] T. Herr, K. Hartinger, J. Riemensberger, C. Y. Wang, E. Gavartin, R. Holzwarth, M. L. Gorodetsky, and T. J. Kippenberg, Universal formation dynamics and noise of kerr-frequency combs in microresonators, *Nat. Photonics* **6**, 480 (2012).
- [10] D. T. Spencer *et al.*, An optical-frequency synthesizer using integrated photonics, *Nature (London)* **557**, 81 (2018).
- [11] B. Shen *et al.*, Integrated turnkey soliton microcombs, *Nature (London)* **582**, 365 (2020).
- [12] B. Stern, X. Ji, Y. Okawachi, A. L. Gaeta, and M. Lipson, Battery-operated integrated frequency comb generator, *Nature (London)* **562**, 401 (2018).
- [13] S.-W. Huang, J. Yang, S.-H. Yang, M. Yu, D.-L. Kwong, T. Zhevinsky, M. Jarrahi, and C. W. Wong, Globally Stable Microresonator Turing Pattern Formation For Coherent High-Power THz Radiation On-Chip, *Phys. Rev. X* **7**, 041002 (2017).
- [14] B. Yao *et al.*, Gate-tunable frequency combs in graphene–nitride microresonators, *Nature (London)* **558**, 410 (2018).
- [15] Q.-F. Yang, X. Yi, K. Y. Yang, and K. Vahala, Counter-propagating solitons in microresonators, *Nat. Photonics* **11**, 560 (2017).
- [16] X. Xue, Y. Xuan, Y. Liu, P.-H. Wang, S. Chen, J. Wang, D. E. Leaird, M. Qi, and A. M. Weiner, Mode-locked dark pulse kerr combs in normal-dispersion microresonators, *Nat. Photonics* **9**, 594 (2015).
- [17] M. Yu, J. K. Jang, Y. Okawachi, A. G. Griffith, K. Luke, S. A. Miller, X. Ji, M. Lipson, and A. L. Gaeta, Breather soliton dynamics in microresonators, *Nat. Commun.* **8**, 14569 (2017).
- [18] X. Yi, Q.-F. Yang, X. Zhang, K. Y. Yang, X. Li, and K. Vahala, Single-mode dispersive waves and soliton microcomb dynamics, *Nat. Commun.* **8**, 14869 (2017).
- [19] M. Karpov, M. H. P. Pfeiffer, H. Guo, W. Weng, J. Liu, and T. J. Kippenberg, Dynamics of soliton crystals in optical microresonators, *Nat. Phys.* **15**, 1071 (2019).
- [20] T. E. Drake, J. R. Stone, T. C. Briles, and S. B. Papp, Thermal decoherence and laser cooling of kerr microresonator solitons, *Nat. Photonics* **14**, 480 (2020).
- [21] M.-G. Suh, Q.-F. Yang, K. Y. Yang, X. Yi, and K. J. Vahala, Microresonator soliton dual-comb spectroscopy, *Science* **354**, 600 (2016).
- [22] X. Ji, X. Yao, A. Klenner, Y. Gan, A. L. Gaeta, C. P. Hendon, and M. Lipson, Chip-based frequency comb sources for optical coherence tomography, *Opt. Express* **27**, 19896 (2019).
- [23] P. J. Marchand, J. Riemensberger, J. C. Skehan, J. Ho, M. H. P. Pfeiffer, J. Liu, C. Hauger, T. Lasser, and T. J. Kippenberg, Soliton microcomb based spectral domain optical coherence tomography, *Nat. Commun.* **12**, 427 (2021).
- [24] S.-W. Huang, J. Yang, M. Yu, B. H. McGuyer, D.-L. Kwong, T. Zhevinsky, and C. W. Wong, A broadband chip-scale optical frequency synthesizer at 2.7×10^{-16} relative uncertainty, *Sci. Adv.* **2**, e1501489 (2016).
- [25] J. Kiessling, I. Breunig, P. G. Schunemann, K. Buse, and K. L. Vodopyanov, High power and spectral purity continuous-wave photonic thz source tunable from 1 to 4.5 THz for nonlinear molecular spectroscopy, *New J. Phys.* **15**, 105014 (2013).
- [26] Y.-S. Jang, H. Liu, J. Yang, M. Yu, D.-L. Kwong, and C. W. Wong, Nanometric Precision Distance Metrology Via Hybrid Spectrally Resolved And Homodyne Interferometry In A Single Soliton Frequency Microcomb, *Phys. Rev. Lett.* **126**, 023903 (2021).
- [27] J. Riemensberger, A. Lukashchuk, M. Karpov, W. Weng, E. Lucas, J. Liu, and T. J. Kippenberg, Massively parallel coherent laser ranging using a soliton microcomb, *Nature (London)* **581**, 164 (2020).

- [28] J. Feldmann *et al.*, Parallel convolutional processing using an integrated photonic tensor core, *Nature (London)* **589**, 52 (2021).
- [29] X. Xu *et al.*, 11 tops photonic convolutional accelerator for optical neural networks, *Nature (London)* **589**, 44 (2021).
- [30] P. Marin-Palomo *et al.*, Microresonator-based solitons for massively parallel coherent optical communications, *Nature (London)* **546**, 274 (2017).
- [31] A. Fülöp *et al.*, High-order coherent communications using mode-locked dark-pulse kerr combs from microresonators, *Nat. Commun.* **9**, 1598 (2018).
- [32] B. Corcoran *et al.*, Ultra-dense optical data transmission over standard fibre with a single chip source, *Nat. Commun.* **11**, 2568 (2020).
- [33] T. J. Kippenberg, A. L. Gaeta, M. Lipson, and M. L. Gorodetsky, Dissipative kerr solitons in optical microresonators, *Science* **361**, eaan8083 (2018).
- [34] D. C. Cole, E. S. Lamb, P. Del'Haye, S. A. Diddams, S. B. Papp, P. Del'Haye, S. A. Diddams, and S. B. Papp, Soliton crystals in kerr resonators, *Nat. Photonics* **11**, 671 (2017).
- [35] Z. Lu *et al.*, Synthesized soliton crystals, *Nat. Commun.* **12**, 3179 (2021).
- [36] J. Hu, J. He, J. Liu, A. S. Raja, M. Karpov, A. Lukashchuk, T. J. Kippenberg, and C.-S. Brès, Reconfigurable radiofrequency filters based on versatile soliton microcombs, *Nat. Commun.* **11**, 4377 (2020).
- [37] X. Yi, Q.-F. Yang, K. Vahala, and K. Y. Yang, Active capture and stabilization of temporal solitons in microresonators, *Opt. Lett.* **41**, 2037 (2016).
- [38] T. Herr, V. Brasch, J. D. Jost, C. Y. Wang, N. M. Kondratiev, M. L. Gorodetsky, and T. J. Kippenberg, Temporal solitons in optical microresonators, *Nat. Photonics* **8**, 145 (2014).
- [39] H. Zhou, Y. Geng, W. Cui, S. W. Huang, Q. Zhou, K. Qiu, and C. Wei Wong, Soliton bursts and deterministic dissipative kerr soliton generation in auxiliary-assisted microcavities, *Light Sci. Appl.* **8**, 1 (2019).
- [40] Y. Zhao *et al.*, Soliton burst and bi-directional switching in the platform with positive thermal-refractive coefficient using an auxiliary laser, *Laser Photon. Rev.* **15**, 2100264 (2021).
- [41] S.-W. Huang, H. Liu, J. Yang, M. Yu, D.-L. Kwong, and C. W. Wong, Smooth and flat phase-locked kerr frequency comb generation by higher order mode suppression, *Sci. Rep.* **6**, 26255 (2016).
- [42] Y. Li *et al.*, Real-time transition dynamics and stability of chip-scale dispersion-managed frequency microcombs, *Light Sci. Appl.* **9**, 52 (2020).
- [43] E. Lucas, H. Guo, J. D. Jost, M. Karpov, and T. J. Kippenberg, Detuning-dependent properties and dispersion-induced instabilities of temporal dissipative kerr solitons in optical microresonators, *Phys. Rev. A* **95**, 043822 (2017).
- [44] X. Jiang and L. Yang, Optothermal dynamics in whispering-gallery microresonators, *Light Sci. Appl.* **9**, 24 (2020).
- [45] H. Guo, M. Karpov, E. Lucas, A. Kordts, M. H. P. Pfeiffer, V. Brasch, G. Lihachev, V. E. Lobanov, M. L. Gorodetsky, and T. J. Kippenberg, Universal dynamics and deterministic switching of dissipative kerr solitons in optical microresonators, *Nat. Phys.* **13**, 94 (2017).
- [46] Ó. B. Helgason, F. R. Arteaga-Sierra, Z. Ye, K. Twayana, P. A. Andrekson, M. Karlsson, J. Schröder, and V. Torres-Company, Dissipative solitons in photonic molecules, *Nat. Photonics* **15**, 305 (2021).